Journal of Scientific Computing, Vol. 32, No. 1, July 2007 (© 2006)
DOI: 10.1007/s10915-006-9118-4

The Approximation and Computation of a Basis of the Trace Space $H^{1/2}$

Petr Klouček,[1,2,5] Danny C. Sorensen,[3] and Jennifer L. Wightman[4]

Received June 22, 2006; accepted (in revised form) September 21, 2006; Published online December 7, 2006

We present a method for construction of an approximate basis of the trace space $H^{1/2}$ based on a combination of the Steklov spectral method and a finite element approximation. Specifically, we approximate the Steklov eigenfunctions with respect to a particular finite element basis. Then solutions of elliptic boundary value problems with Dirichlet boundary conditions can be efficiently and accurately expanded in the discrete Steklov basis. We provide a reformulation of the discrete Steklov eigenproblem as a generalized eigenproblem that we solve by the implicitly restarted Arnoldi method of ARPACK. We include examples highlighting the computational properties of the proposed method for the solution of elliptic problems on bounded domains using both a conforming bilinear finite element and a non-conforming harmonic finite element. In addition, we document the efficiency of the proposed method by solving a Dirichlet problem for the Laplace equation on a densely perforated domain.

KEY WORDS: Steklov eigenvalues problem; generalized eigenvalue problem; trace spaces; elliptic PDEs.

[1] Texas Learning and Computational Center, University of Houston, 4800 Calhoun, TX 77204, USA.
[2] Institut de Mathèmatiques, Universitè de Neuchâtel, Rue Emile Argand 11, CH-2007 Neuchâtel, Switzerland. E-mail: kloucek@mac.com
[3] Department of Computational and Applied Math, Rice University, 6100 Main Street, Houston, TX 77005, USA. E-mail: sorensen@rice.edu
[4] Department of Math and Statistics, Coastal Carolina University, P.O. Box 261954, Conway, SC 29528, USA. E-mail: wightman@coastal.edu
[5] To whom correspondence should be addressed. E-mail: kloucek@mac.com

1. INTRODUCTION

The purpose of this paper is to present a technique for solving the elliptic problem

$$\begin{aligned} -\nabla \cdot (\boldsymbol{a}(x)\nabla u(x)) &= 0 \quad \text{in } \Omega, \\ u &= g \quad \text{on } \partial\Omega \end{aligned} \tag{1.1}$$

by combining a finite element approximation of the elliptic operator with the Steklov spectral method developed by Auchmuty [1]. As we will outline in Sec. 2, the solution can be represented in the form

$$u(x) = \sum_{j=0}^{\infty} c_j u^j(x) \qquad \text{with} \quad c_j = (1+\delta_j) \int_{\partial\Omega} \rho(s) g(s) T u^j(s)\, dS \quad \text{for } j \geqslant 0,$$

where $\{(\delta_j, u^j)\}_{j=0}^{\infty}$ denotes the family of eigenpairs for the Steklov eigenproblem associated with (1.1). Here, T denotes the trace operator $H^1(\Omega) \mapsto H^{1/2}(\partial\Omega)$, and dS denotes the invariant infinitesimal surface element. We assume the domain Ω is bounded and simply connected having a Lipschitz boundary, and we restrict ourselves to the case $\Omega \subset \mathbb{R}^2$. In two dimensions, dS represents the arc-length along the boundary $\partial\Omega$.

For the sake of simplicity, we present our methodology only for the harmonic Dirichlet problem, i.e., with the coefficient $\boldsymbol{a} = \mathrm{I}$, where I is the identity matrix. The generalization of this approach to coefficients satisfying the following conditions is straightforward:

(i) $\boldsymbol{a}$: $\Omega \mapsto M^{2\times 2}(\mathbb{R})$, $\boldsymbol{a} = \boldsymbol{a}^T$, $\boldsymbol{a} \in L^{\infty}(\Omega, I\!R^{2\times 2})$,

(ii) $\sum_{i,j} \boldsymbol{a}_{i,j}(x)\psi_i\psi_j \geqslant \Lambda_0 |\psi|^2$ for all $\psi \in I\!R^2$, and for a.a. $x \in \Omega$,

(iii) $|a(u, v)| \leqslant \Lambda_1 \|u\|_{H^1(\Omega)} \|v\|_{H^1(\Omega)}$.

Here $a(\cdot, \cdot)$ is the bilinear form corresponding to the weak form of the differential operator appearing in (1.1). Futhermore, the Steklov spectral method can be applied to problems with non-trivial right-hand sides by using linearity (or superposition) and standard methods. We refer to Auchmuty [1] for details.

The outline of this paper is as follows. In Sect. 2, we describe the spectral representation of solutions to (1.1) using Steklov eigenfunctions, a technique developed by Auchmuty [1]. In Sect. 3, we develop the discrete Steklov spectral method using a finite element implementation. The discrete Steklov eigenfunctions are written with respect to the finite element basis, and the discrete Steklov eigenvalues solve a generalized eigenvalue

problem. In Sect. 4, we present the discrete Steklov spectral method solution to (1.1) computed on the unit disk, and in Sect. 5, we present computations performed on a highly perforated domain. Finally, in Sect. 6, we discuss the potential advantages of using the discrete Steklov spectral method and give some possibilities for future work.

2. STEKLOV EIGENPAIRS

Our approach to solving the elliptic problem (1.1) combines the infinite dimensional Steklov spectral representation of the solution $u(x)$ with a finite dimensional finite element implementation. In this section, we describe the spectral representation of $u(x)$ with respect to Steklov eigenfunctions.

First, the harmonic Steklov eigenproblem for a domain Ω is defined to be that of finding non-trivial solutions (δ, u) of the system

$$\begin{aligned} -\Delta u(x) &= 0, & x &\in \Omega, \\ \nabla u(s) \cdot n(s) &= \delta \rho(s) u(s), & s &\in \partial\Omega, \end{aligned} \tag{2.1}$$

where $\rho \in L^\infty(\partial\Omega)$ is positive on $\partial\Omega$ and satisfies $\int_{\partial\Omega} \rho(s)\, dS = 1$. The value δ is the harmonic Steklov eigenvalue, and the function u is the corresponding eigenfunction. The weak form of (2.1) is to find non-trivial (δ, u) in $\mathbb{R} \times H^1(\Omega)$ satisfying

$$\int_\Omega \nabla u(x) \cdot \nabla v(x)\, dx - \delta \int_{\partial\Omega} \rho(s) u(s) v(s)\, dS = 0, \quad \forall v \in H^1(\Omega). \tag{2.2}$$

We observe that $\delta_0 = 0$ is a simple eigenvalue of (2.2) with the associated eigenfunction $u^0 \equiv 1$. Furthermore, substituting $v = u$ in (2.2), demonstrates that the harmonic Steklov eigenvalues are positive.

Auchmuty [1] proves that there exists a countable increasing sequence of eigenvalues with the property that each eigenvalue δ_j has finite multiplicity and $\delta_j \to \infty$ as $j \to \infty$. The jth eigenpair (δ_j, u^j) of (2.1) is constructed using the variational principle

$$\gamma_j \overset{\text{def}}{=} \sup_{u \in \mathcal{B}^j} \int_{\partial\Omega} \rho(s) (Tu(s))^2\, dS, \tag{2.3}$$

where

$$\mathcal{B}^j = \left\{ u \in H^1(\Omega) : \int_\Omega |\nabla u(x)|^2\, dx + \int_{\partial\Omega} \rho(s)\, (Tu(s))^2\, dS \leqslant 1 \text{ and } \int_{\partial\Omega} \rho(s) Tu(s)\, Tu^k(s)\, dS = 0 \text{ for } 0 \leqslant k < j \right\}$$

is a unit ball of $H^1(\Omega)$-functions which are orthogonal to the first j eigenfunctions. The eigenfunction $u^j(x)$ is the maximizer of (2.3) and the corresponding eigenvalue satisfies

$$\delta_j = \frac{1}{\gamma_j} - 1 \quad \text{for } j \geqslant 0. \tag{2.4}$$

This family of eigenfunctions $\{u^j\}_{j=0}^{\infty}$ is orthogonal with respect to the boundary inner product

$$\langle u, v \rangle_\rho \stackrel{\text{def}}{=} \int_{\partial\Omega} \rho(s) Tu(s) Tv(s)\, dS \tag{2.5}$$

and orthonormal with respect to the $\mathcal{F}$-inner product

$$\mathcal{F}(u, v) \stackrel{\text{def}}{=} \int_\Omega \nabla u(x) \cdot \nabla v(x)\, dx + \int_{\partial\Omega} \rho(s) Tu(s) Tv(s)\, dS, \tag{2.6}$$

which is equivalent to the inner product on $H^1(\Omega)$, [1].

Lemma 2.1. Let $\{(\delta_j, u^j)\}_{j=0}^{\infty}$ denote the family of eigenpairs for the Steklov eigenproblem (2.1). Then

$$\langle u^j, u^k \rangle_\rho = \int_{\partial\Omega} \rho(s) Tu^j(s) Tu^k(s)\, dS = \frac{1}{1+\delta_j} \delta_{jk} \tag{2.7}$$

and

$$\mathcal{F}(u^j, u^k) = \int_\Omega \nabla u^j(x) \cdot \nabla u^k(x)\, dx + \int_{\partial\Omega} \rho(s) Tu^j(s) Tu^k(s)\, dS = \delta_{jk}. \tag{2.8}$$

The proof of this lemma is straightforward and left to the reader. We point out that, according to Lemma 2.1, the eigenfunctions are *orthonormal* with respect to the $\mathcal{F}$-inner product on $H^1(\Omega)$, but they are merely orthogonal on the boundary $\partial\Omega$. However, with a simple scaling of the eigenfunctions, we can achieve orthonormality on the boundary while sacrificing the orthonormality in the interior. Namely, let us rescale each eigenfunction u^j by $\sqrt{1+\delta_j}$, and let us define $v^j(x) = \sqrt{1+\delta_j}\, u^j(x)$. Then it is easy to show that

$$\langle v^j, v^k \rangle_\rho = \delta_{jk}$$

and

$$\mathcal{F}(v^j, v^k) = \frac{\delta_{jk}}{(1+\delta_j)}.$$

We will see in the next section, that the computed discrete eigenfunctions are orthonormal on the boundary $\partial\Omega$, and we are careful to distinguish between the computed eigenfunctions $\{v_h^j\}$ and the corresponding eigenfunctions $\{u_h^j\}$ that are orthonormal in the interior of Ω. The difference in orthonormality arises from the construction of the eigenfunctions, and essentially, one is free to choose between $\mathcal{F}$-orthonormality and ρ-orthonormality.

In the context of this section, it is the $\mathcal{F}$-orthonormality of the eigenfunctions $\{u_h^j\}$ that provides the link between the Steklov eigenvalue problem (2.1) and the elliptic problem (1.1), as we discuss presently. Let us denote by $H_{\mathcal{F}}(\Omega)$ the subspace of $H^1(\Omega)$ that is $\mathcal{F}$-orthogonal to $H_0^1(\Omega)$. Then we obtain the decomposition

$$H^1(\Omega) = H_0^1(\Omega) \oplus_{\mathcal{F}} H_{\mathcal{F}}(\Omega).$$

The fundamental result upon which the Steklov spectral method is based is that the $\mathcal{F}$-orthonormal harmonic Steklov eigenfunctions $\{u^j\}_{j=0}^{\infty}$ provide a basis for the space $H_{\mathcal{F}}(\Omega)$ [Theorem 7.3, [1]].

Returning to the elliptic problem (1.1), the weak form reads as follows: find $u \in H^1(\Omega)$, $u = g$ on $\partial\Omega$ in the sense of traces, such that

$$\int_{\Omega} \nabla u(x) \nabla \varphi(x)\, dx = 0, \quad \forall \varphi \in H_0^1(\Omega).$$

In other words, $u \in H^1(\Omega)$ satisfies

$$\mathcal{F}(u, \varphi) = 0, \quad \forall \varphi \in H_0^1(\Omega).$$

Hence, the solution u is in $H_{\mathcal{F}}(\Omega)$, and we can represent u in terms of the Steklov $H_{\mathcal{F}}(\Omega)$-basis. We point out that the trace space $H^{1/2}(\partial\Omega)$ consists of all functions g for which this weak formulation has a solution. Since the trace of the solution $u \in H_{\mathcal{F}}(\Omega)$ is equal to $g \in H^{1/2}(\partial\Omega)$, we can identify $H^{1/2}(\partial\Omega)$ with $H_{\mathcal{F}}(\Omega)$. Furthermore, the Steklov eigenfunctions provide a basis for $H^{1/2}(\partial\Omega)$ in the sense of traces.

Now, we represent the solution $u(x)$ in terms of the Steklov $H_{\mathcal{F}}(\Omega)$-basis functions as follows:

$$u(x) = \sum_{i=0}^{\infty} c_j u^j(x) \tag{2.9}$$

for some coefficients c_j yet to be determined. By the compactness of the trace operator T, the trace of u on $\partial\Omega$ is given by

$$Tu = \sum_{j=0}^{\infty} c_j T u^j. \tag{2.10}$$

Multiplying (2.10) by $\rho T u^k$ and integrating over $\partial\Omega$ yields, in view of the orthogonality (2.7), the following formula for the coefficients c_j

$$c_j = (1+\delta_j)\langle g, Tu^j\rangle_\rho \quad \text{for } j \geqslant 0. \tag{2.11}$$

At this point we have a complete expression for the Steklov spectral representation of the solution $u(x)$ to the elliptic problem (1.1). We summarize the above exposition in the following theorem (see also Auchmuty [Theorem 9.1, 1]).

Theorem 2.2. Let us consider the elliptic problem (1.1) with the coefficient $\boldsymbol{a} = \mathrm{I}$. Let $\{(\delta_j, u^j)\}_{j=0}^{\infty}$ denote the family of eigenpairs for the Steklov eigenproblem (2.1). Then problem (1.1) is uniquely solvable if and only if

$$\sum_{j=0}^{\infty} (1+\delta_j)^2 \left(\int_{\partial\Omega} \rho(s) g(s) T u^j(s)\, dS \right)^2 < \infty. \tag{2.12}$$

Moreover, the solution is given by

$$u(x) = \sum_{j=0}^{\infty} c_j u^j(x) \qquad \text{with} \quad c_j = (1+\delta_j) \int_{\partial\Omega} \rho(s) g(s) T u^j(s)\, dS \quad \text{for } j \geqslant 0. \tag{2.13}$$

In addition, let $u_m \overset{\text{def}}{=} \sum_{j=0}^{m} c_j u^j(x)$. Then

$$\|u - u_m\|_{L^2(\partial\Omega),\rho} \leqslant (1+\delta_{m+1})^{-1/2} \|g\|_{H^{1/2}(\partial\Omega),\rho}, \tag{2.14}$$

where δ_{m+1} is the $m+1$-st Steklov eigenvalue. Finally, we have

$$\|u - u_m\|_{H^1(\Omega)} \to 0_+ \tag{2.15}$$

as $m \to +\infty$.

Proof. The representation formula (2.13) was developed in the above outline of the theory. It is easy to show that $\|u\|_{\mathcal{F}}^2 = \sum_{j=0}^{\infty} c_j^2$ using the $\mathcal{F}$-orthonormality of the eigenfunctions. Now, applying Parseval's theorem yields

$$\|u\|_{\mathcal{F}}^2 = \sum_{j=0}^{\infty} \left(1+\delta_j\right)^2 \left|\langle g, Tu^j\rangle_\rho\right|^2.$$

The solvability criterion (2.12) follows since the $\mathcal{F}$-norm is equivalent to the H^1-norm.

We note that (2.12) is a criterion that the boundary data g must satisfy in order for the elliptic problem (1.1) to have a solution. Therefore (2.12) provides a specific condition for a function g to be in the trace space $H^{1/2}(\partial\Omega)$, and we define the norm of $H^{1/2}(\partial\Omega)$ by

$$\|g\|_{H^{1/2}(\partial\Omega),\rho}^2 \stackrel{\text{def}}{=} \sum_{k=0}^{\infty} (1+\delta_k)^2 \left(\int_{\partial\Omega} \rho(s) g(s) Tu^k(s)\, dS\right)^2. \tag{2.16}$$

In addition, the $L^2(\partial\Omega)$ norm can be written as

$$\|g\|_{L^2(\partial\Omega),\rho}^2 = \sum_{k=0}^{\infty} (1+\delta_k) \left(\int_{\partial\Omega} \rho(s) g(s) Tu^k(s)\, dS\right)^2. \tag{2.17}$$

The expression above is obtained directly by taking the L^2-norm of the spectral representation (2.9).

We now turn our attention to the truncation error estimate. We have

$$\begin{aligned} u(x) - u_m(x) &= \sum_{j=m+1}^{\infty} c_j u^j(x) \\ &= \sum_{j=m+1}^{\infty} (1+\delta_j) \int_{\partial\Omega} \rho(s) g(s) Tu^j(s)\, dS\, u^j(x). \end{aligned} \tag{2.18}$$

In view of the orthogonality property (2.7), the expression (2.18), and since the eigenvalues are increasing, we obtain

$$
\begin{aligned}
&\|u-u_m\|^2_{L^2(\partial\Omega),\rho} \\
&\quad = \int_{\partial\Omega} \rho(s)\,(u-u_m)^2\,(s)\,dS \\
&\quad = \sum_{k,j=m+1}^{\infty} (1+\delta_j)(1+\delta_k) \int_{\partial\Omega} \rho(s) u^j(s) u^k(s)\,dS \int_{\partial\Omega} \rho(s) g(s) T u^j(s)\,dS \\
&\qquad \times \int_{\partial\Omega} \rho(s) g(s) T u^k(s)\,dS \\
&\quad \leqslant \frac{1}{1+\delta_{m+1}} \sum_{k=m+1}^{\infty} (1+\delta_k)^2 \left(\int_{\partial\Omega} \rho(s) g(s) T u^j(s)\,dS \right)^2 \\
&\quad \leqslant \frac{1}{1+\delta_{m+1}} \|g\|^2_{H^{1/2}(\partial\Omega),\rho}\,.
\end{aligned}
$$

The convergence result (2.15) follows from the expression for the H^1-norm in terms of the Steklov spectra. Namely,

$$
\begin{aligned}
\|u-u_m\|^2_{H^1(\Omega)} \leqslant C\,\|u-u_m\|^2_{\mathcal{F}} &= \sum_{j=m+1}^{\infty} c_j^2 \\
&= \sum_{j=m+1}^{\infty} (1+\delta_j)^2 \left(\int_{\partial\Omega} \rho(s) g(s) T u^j(s)\,dS \right)^2 .
\end{aligned}
\tag{2.19}
$$

Since the last expression in (2.19) is the remainder of the $H^{1/2}(\partial\Omega)$-norm of g which is finite, we have

$$
\sum_{j=m+1}^{\infty} (1+\delta_j)^2 \left(\int_{\partial\Omega} \rho(s) g(s) T u^j(s)\,dS \right)^2 \to 0_+ \quad \text{as } m \to +\infty.
$$

The proof is completed. □

3. FINITE ELEMENT IMPLEMENTATION

In this section, we derive the discrete Steklov spectral method by combining the Steklov spectral method of Sec. 2 with a finite element approximation. First, we will define two different finite element spaces that will be considered in this paper. Then in Sec. 3.1, we show that the discrete Steklov eigenfunctions, which are written with respect to the finite element basis, solve a discrete generalized eigenvalue problem, and in Sec. 3.2, we develop a compact formula for the expansion coefficients.

In Sec. 3.3, we prove that the eigenfunctions obtained from the generalized eigenproblem satisfy a discrete version of the variational principle (2.3). Finally, in Sec. 3.4, we explain why the number of discrete eigenpairs that can be obtained depends on the mesh size h of the discretization.

For the purposes of this paper, we consider two different finite element approximations for the elliptic problem (1.1): a conforming bilinear approximation and a non-conforming harmonic approximation. First, we prescribe a rectangular partition τ_h of the domain Ω, assumed to have a polygonal boundary. Let the parent element be the rectangle $R \stackrel{\text{def}}{=} [a-r, a+r] \times [b-s, b+s]$ with center (a, b) and edge lengths $2r$ and $2s$. Then the finite element space for the bilinear approximation is given by

$$V_{Q_1} \stackrel{\text{def}}{=} \Big\{ v_h \in H^1(\Omega) : v_h\big|_R \in \text{span}\{1, x, y, xy\}, \\ \times \forall R \in \tau_h; \quad v_h \text{ is continuous at mesh vertices} \Big\}.$$

The finite element space for the non-conforming harmonic approximation studied by Klouček *et al.* [11] is given by

$$V_{P_h} \stackrel{\text{def}}{=} \left\{ v_h \in L^2(\Omega) : v_h\big|_R \in \text{span}\left\{1,\ x,\ y,\ \left(\frac{x}{r}\right)^2 - \left(\frac{y}{s}\right)^2\right\},\ \forall R \in \tau_h; \right. \\ \left. \int_F v_h\big|_{R'}\, dS = \int_F v_h\big|_{R''}\, dS,\ \forall \text{ faces } F = \partial R' \cap \partial R'' \neq \emptyset,\ R', R'' \in \tau_h \right\}.$$

For a definition of the usual norm and seminorm for the space V_{P_h}, see Klouček *et al.* [11].

For simplicity of notation, we use V_h to denote either of the finite element spaces V_{Q_1} or V_{P_h} when a distinction between the two spaces is not required. Then we will say V_h is an N_h-dimensional space with basis functions $\{\phi_j(x)\}_{j=1}^{N_h}$. In addition, we define the *boundary layer* of the partition τ_h to be the index set of basis functions having non-trivial support on $\partial\Omega$. We denote this index set by $\mathcal{J}_b$ and define $M_h \stackrel{\text{def}}{=} \dim \mathcal{J}_b$. For the finite element space V_{Q_1}, we have

$$\mathcal{J}_b = \{i : \text{the vertex } x_i \in \partial\Omega\},$$

whereas for V_{P_h},

$$\mathcal{J}_b = \{i : \text{the face } F_i \in \partial R \text{ for some element } R \cap \partial\Omega \neq \emptyset\}.$$

For convenience, we can renumber the basis functions so that $\mathcal{J}_b = \{1, \ldots, M_h\}$. The dimension of the boundary layer becomes relevant when we consider the number of discrete eigenfunctions that can be obtained for a particular mesh size h, a topic we discuss in depth in Sec. 3.4.

The objective of this paper is to find an approximate solution $u_h(x)$ to the elliptic problem (1.1) using discrete Steklov eigenfunctions. First we obtain the discrete Steklov eigenfunctions $\{u_h^j\}$ by solving the discrete version of the Steklov weak formulation (2.2). Then we represent the solution u_h of (1.1) as an expansion of discrete eigenfunctions in a manner similar to that described in Theorem 2.2. We call this technique the discrete Steklov spectral method, and we describe this method in detail throughout the following sections.

3.1. The Generalized Eigenvalue Problem

Recall from Sec. 2 that the Steklov eigenpair $\{\delta_j, u^j\}$ solved the weak formulation (2.2) of the Steklov eigenproblem (2.1). Furthermore, the eigenfunctions satisfied the orthogonality condition (2.7). Similarly, we define the discrete Steklov eigenpair $\{\delta_h^j, u_h^j\}$ to solve the discrete weak formulation

$$\int_\Omega \nabla u_h^j(x) \cdot \nabla v_h(x)\, dx - \delta_h^j \int_{\partial\Omega} \rho(s)\, u_h^j(s)\, v_h(s)\, dS = 0, \quad \forall v_h \in V_h \tag{3.1}$$

and satisfy the orthogonality condition

$$\int_{\partial\Omega} \rho(s)\, Tu_h^j(s)\, Tu_h^k(s)\, dS = \frac{\delta_{jk}}{1+\delta_h^j}. \tag{3.2}$$

We represent the discrete eigenfunction $u_h^j \in V_h$ with respect to the finite element basis of V_h. That is,

$$u_h^j(x) = \sum_{i=1}^{N_h} q_i^j \phi_i(x), \tag{3.3}$$

where $q^j = \left\{q_i^j\right\}_{i=1}^{N_h}$ is the coordinate vector of u_h^j. Now, substituting (3.3) into the weak formulation (3.1) and testing by each basis function $\phi_i(x)$, we obtain the following linear system of equations:

$$Aq^j - \delta_h^j B q^j = 0, \tag{3.4}$$

where A and B are $N_h \times N_h$ matrices defined by

$$A_{ij} = \int_\Omega \nabla\phi_i(x) \cdot \nabla\phi_j(x)\, dx \qquad \text{and} \quad B_{ij} = \int_{\partial\Omega} \rho(s)\, T\phi_i(s)\, T\phi_j(s)\, dS.$$

We note that both A and B are sparse matrices. Moreover, $\text{rank}(B) = M_h$ since the ith row of B is non-zero only if $i \in \mathcal{J}_b$. Finally, Eq. (3.4) can be written in the form of a generalized eigenproblem as follows:

$$AQ = BQD. \tag{3.5}$$

Here, Q is an $N_h \times M_h$ matrix, where the jth column of Q is the coordinate vector q^j corresponding to the jth discrete eigenfunction u_h^j. In addition, D is a diagonal matrix such that $D_{jj} = \delta_h^j$.

The advantage to the generalized eigenproblem formulation is that we can compute the dominant portion of the spectrum and all the corresponding eigenvectors simultaneously by application of the *Implicitly Restarted Arnoldi Method* [16]. In practice, we solve (3.5) using the ARPACK library[1] written by Lehoucq *et al.* [13]. Specifically, given matrices A and B as input, ARPACK outputs the eigenvalue matrix D, and an eigenfunction matrix $\tilde{Q}$ that differs from Q in the scaling of the eigenfunctions.

The difference in scaling between the Q- and $\tilde{Q}$-eigenfunctions is tied directly to the orthogonality of eigenfunctions. A feature of ARPACK is that the eigenfunctions it produces satisfy the orthogonality condition $\tilde{Q}^T B \tilde{Q} = I$. Therefore, if we define the discrete eigenfunction

$$v_h^j(x) \stackrel{\text{def}}{=} \sum_{i=1}^{N_h} \tilde{q}_i^j \phi_i(x)$$

then v_h^j satisfies

$$\left(\tilde{q}^j\right)^T B \tilde{q}^k = \int_{\partial\Omega} \rho(s)\, T v_h^j(s)\, T v_h^k(s)\, dS = \delta_{jk}.$$

In order to obtain compatibility between v_h^j and the desired eigenfunction u_h^j that satisfies (3.2), we apply the scaling

$$u_h^j(x) = \frac{1}{\sqrt{1+\delta_h^j}} v_h^j(x).$$

[1]The software is available at www.caam.rice.edu/software/ARPACK/

This distinction between the computed eigenfunction v_h^j and the discrete counterpart u_h^j of the eigenfunctions described in Sec. 2 also affects the way we compute the coefficients for the expansion of u_h using Steklov eigenfunctions, as we discuss now.

3.2. Calculation of the Expansion Coefficients

As stated, our overall goal in this paper is to approximate the solution $u_h(x)$ of the elliptic problem (1.1) using discrete Steklov eigenfunctions. Namely, we write

$$u_h(x) = \sum_{j=1}^{M_h} c_j u_h^j(x), \tag{3.6}$$

where each eigenfunction u_h^j satisfies the orthogonality condition (3.2). Just as in Sec. 2, the coefficients in Eq. (3.6) are given by the formula

$$c_j = (1+\delta_h^j) \int_{\partial\Omega} \rho(s)\, g(s)\, T u_h^j(s)\, dS.$$

Maintaining the convention that v_h^j is an approximate eigenfunction and $v_h^j(x) = \sqrt{1+\delta_h^j}\, u_h^j(x)$, we may write

$$\begin{aligned} u_h(x) &= \sum_{j=1}^{M_h} \frac{c_j}{\sqrt{1+\delta_h^j}} v_h^j(x) = \sum_{j=1}^{M_h} \sqrt{1+\delta_h^j} \int_{\partial\Omega} \rho(s)\, g(s)\, T u_h^j(s)\, dS \\ &= \sum_{j=1}^{M_h} \int_{\partial\Omega} \rho(s)\, g(s)\, T v_h^j(s)\, dS = \sum_{j=1}^{M_h} w_j v_h^j(x). \end{aligned}$$

Therefore, the expansion coefficients with respect to the calculated eigenfunctions are defined by

$$w_j = \int_{\partial\Omega} \rho(s)\, g(s)\, T v_h^j(s)\, dS. \tag{3.7}$$

We now develop a compact formula for the coefficient w_j that does not require any integration.

We see that the expansion coefficients depend on the Dirichlet boundary data g of the elliptic problem. First, we compute the projection of g

onto the finite element space V_h. That is, we write

$$g_h(s) = \sum_{i=1}^{M_h} G_i \varphi_i(s), \tag{3.8}$$

where $G = \{G_i\}_{i=1}^{M_h}$ is the coordinate vector for $g_h(s)$. In other words, the Dirichlet boundary datum for the finite element discretization is not obtained by an interpolation of g but rather by the L^2-projection of g onto the trace space of the considered finite element space.

Without loss of generality, we have assumed that the M_h degrees of freedom (vertices or faces) in the boundary layer are indexed $1, \ldots, M_h$. Based on this convention, we define $\tilde{B}$ to be the $M_h \times M_h$ submatrix of B consisting of all non-zero rows and columns of B, i.e., $\tilde{B} = B(1:M_h, 1:M_h)$. Now multiplying both sides of Eq. (3.8) by ϕ_j and integrating over $\partial\Omega$, we obtain

$$F_j \stackrel{\text{def}}{=} \int_{\partial\Omega} \rho(s)\, g(s)\, T\phi_j(s)\, dS = \sum_{i=1}^{M_h} G_i \int_{\partial\Omega} \rho(s)\, T\phi_i(s)\, T\phi_j(s)\, dS = \tilde{B}(j,:)G$$

for $j = 1, \ldots, M_h$. We can now solve the system of equations $F = \tilde{B}G$ for the coordinate vector G. We note that the matrix $\tilde{B}$ is invertible since $x^T \tilde{B} x$ is the discrete inner product corresponding to $\langle \cdot, \cdot \rangle_\rho$.

Referring back to formula (3.7), we can now write the vector of coefficients $W = \{w_j\}_{j=1}^{M_h}$ in the form

$$W = G^T \tilde{B} \tilde{Q}_T.$$

Here $\tilde{Q}$ is the eigenfunction matrix produced by ARPACK, and $\tilde{Q}_T$ is defined to be the submatrix $\tilde{Q}(1:M_h, 1:M_h)$. Essentially, $\tilde{Q}_T$ represents the trace of $\tilde{Q}$ on the boundary $\partial\Omega$ in the discrete sense. Finally, we arrive at the discrete Steklov spectral expansion

$$u_h(x) = \sum_{j=1}^{M_h} \sum_{i=1}^{N_h} w_j \tilde{q}_i^j \phi_i(x) \tag{3.9}$$

that solves the Laplace equation with Dirichlet boundary function g.

3.3. The Discrete Variational Principle

In this section, we make the connection between the discrete Steklov eigenfunctions calculated in Sec. 3.1 and the variational principle

(2.3) used to calculate the classical Steklov eigenfunctions in Sec. 2. We define the discrete version of the space $\mathcal{B}^j$ by

$$\mathcal{B}_h^j \stackrel{\text{def}}{=} \left\{ u_h^j(x) = \sum_{i=1}^{N_h} q_i^j \phi_i(x) : \left(q^j\right)^T A q^j + \left(q^j\right)^T B q^j \leqslant 1 \text{ and } \left(q^j\right)^T B q^k = 0 \text{ for } 0 \leqslant j < k \leqslant \dim \mathcal{J}_b \right\}.$$

Then we have the following result.

Lemma 3.1. Let the discrete Steklov eigenpair $\{(\delta_j, q^j)\}$ be given by the solution of the generalized eigenproblem

$$AQ = BQD,$$

where the jth eigenvector q^j is the jth column of Q. Then the eigenfunction $u_h^j(x) = \sum_{i=1}^{N_h} q_i^j \phi_i(x)$ maximizes the discrete variational principle

$$\gamma_j \stackrel{\text{def}}{=} \max_{u_h \in \mathcal{B}_h^j} \int_{\partial\Omega} \rho(s)\, u_h(s)^2\, dS \tag{3.10}$$

and $\gamma_j = \frac{1}{1+\delta_j}$. Furthermore, if the eigenvectors are scaled so that

$$\left(q^j\right)^T B q^j = \frac{1}{1+\delta_j}$$

then the eigenpair $\left(\delta_j, u_h^j\right)$ satisfies the orthogonality condition (3.2) for $0 \leqslant j < k \leqslant M_h$.

In order to prove Lemma 3.1, we need two simple results.

Lemma 3.2. Let $A, B \in \mathbb{R}^{n\times n}$ be symmetric, where B be positive semi-definite, and assume that $A + \sigma B$ is a regular pencil. Furthermore, suppose that the pair (A, B) has k finite generalized eigenvalues collected in the diagonal matrix Λ and that

$$AQ = BQ\Lambda, \tag{3.11}$$

where the corresponding eigenvectors form the columns of the matrix Q. Then the matrix $Q^T B Q$ is diagonal and positive definite.

Proof. Since B is a semi-definite matrix, there exists a factorization $B = LL^T$, where $L \in \mathbb{R}^{n\times m}$ is some rectangular matrix of rank $m \leqslant n$. We assume that $A + \sigma B$ is a regular pencil. Therefore, there exists a scalar σ_0 such that $A + \sigma_0 B$ is non-singular. It follows from (3.11) that

$$(A + \sigma_0 B)Q = BQ(\Lambda + \sigma_0 I).$$

The matrix $\Lambda + \sigma_0 I$ must be non-singular since $A + \sigma_0 B$ is non-singular. Thus, we may write

$$Q(\Lambda + \sigma_0 I)^{-1} = (A + \sigma_0 B)^{-1} LL^T Q \tag{3.12}$$

and then, multiplying both sides by L^T, we obtain

$$\left(L^T Q\right)(\Lambda + \sigma_0 I)^{-1} = \left(L^T (A + \sigma_0 B)^{-1} L\right) L^T Q.$$

Equation (3.12) may be used to verify that none of the columns of $L^T Q$ are zero, and therefore, the columns of the matrix $L^T Q$ are eigenvectors of the symmetric matrix $\left(L^T (A + \sigma_0 B)^{-1} L\right)$. Consequently, $\left(L^T Q\right)^T \left(L^T Q\right) = Q^T LL^T Q = Q^T BQ$ must be a diagonal matrix. Moreover, $\beta_j = e_j^T Q^T BQ e_j = \|L^T Q e_j\|^2 > 0$. □

Lemma 3.3. Assume that the first hypothesis of Lemma 3.1 holds. In addition, assume that the columns of Q have been normalized so that $Q^T BQ = I$. Then, the eigenvectors $q_i = Q(:, i)$ obey

$$q_i = \operatorname{argmin}\left\{q^T Aq + q^T Bq \mid q^T Bq = 1,\ q^T Bq_j = 0,\ 1 \leqslant j < i\right\}. \tag{3.13}$$

In particular (3.13) yields

$$\begin{aligned} &\gamma_i = \tfrac{1}{1+\delta_i} = \max\left\{q^T Bq \mid q \in \mathcal{B}^i\right\}, \text{ where,} \\ &\mathcal{B}^i \stackrel{\text{def}}{=} \left\{q \in \mathbb{R}^n \mid q^T Aq + q^T Bq \leqslant 1,\ q^T Bq_j = 0,\ 1 \leqslant j < i\right\}. \end{aligned} \tag{3.14}$$

Proof. Since $A + B$ is a symmetric positive definite matrix, there exists a non-singular matrix L such that $A + B = LL^T$. Thus, $AQ = BQD$ can be written in the following form:

$$\begin{aligned} (A + B)Q &= BQ(I + D), \\ LL^T Q &= BL^{-T}(L^T Q)(I + D), \\ (L^T Q)(I + D)^{-1} &= (L^{-1} BL^{-T})(L^T Q). \end{aligned}$$

Hence, the columns of $L^T Q$ are eigenvectors of the symmetric positive semi-definite matrix $L^{-1}BL^{-T}$ with corresponding eigenvalues $\gamma_i = \frac{1}{1+\delta_i}$. We define Γ to be the diagonal matrix with $\Gamma_{ii} = \gamma_i$ and we define the matrix Z as $Z = L^T Q$. It is well known that

$$L^{-1}BL^{-T} = Z\Gamma Z^T,$$

where $Z^T Z = I$. Moreover, using the Courant–Fischer minimax principle we have

$$\gamma_1 = \max_{z \neq 0} \frac{z^T L^{-1} B L^{-T} z}{z^T z} = \max_{q \neq 0} \frac{q^T B q}{q^T L L^T q}$$

and

$$\gamma_i = \max_{\substack{z \neq 0 \\ z^T z_j = 0,\ j<i}} \frac{z^T L^{-1} B L^{-T} z}{z^T z} = \max_{\substack{q \neq 0 \\ q^T L L^T q_j = 0,\ j<i}} \frac{q^T B q}{q^T L L^T q}.$$

Since $LL^T = A + B$, it follows that

$$\begin{aligned} \gamma_i &= \max \left\{ q^T B q \,|\, q^T (A+B) q = 1,\ q^T B q_j = 0,\ 1 \leqslant j < i \right\} \\ &= \max \left\{ q^T B q \,|\, q^T A q + q^T B q \leqslant 1,\ q^T B q_j = 0,\ 1 \leqslant j < i \right\}, \end{aligned} \tag{3.15}$$

which proves (3.14). The eigenvector corresponding to γ_i is obtained as follows:

$$\begin{aligned} q_i &= \operatorname*{argmax}_{\substack{q \neq 0 \\ q^T L L^T q_j = 0,\ j<i}} \frac{q^T B q}{q^T L L^T q} = \operatorname*{argmax}_{\substack{q \neq 0 \\ q^T (A+B) q_j = 0,\ j<i}} \frac{q^T B q}{q^T (A+B) q} \\ &= \operatorname*{argmin}_{\substack{q \neq 0 \\ q^T (A+B) q_j = 0,\ j<i}} \frac{q^T (A+B) q}{q^T B q}. \end{aligned} \tag{3.16}$$

The result (3.13) follows directly from the last part of (3.16). □

Proof. (Of Lemma 3.1) First, we note that

$$\begin{aligned} &\max_{u_h \in \mathcal{B}_h^j} \int_{\partial\Omega} \rho(s)\, u_h(s)^2\, dS \\ &\quad = \max_{q \in \mathcal{B}^j} \sum_{i,k=1}^{N_h} q_i q_k \int_{\partial\Omega} \rho(s)\, \phi_i(s)\, \phi_k(s)\, dS = \max_{q \in \mathcal{B}^j} q^T B q^j. \end{aligned}$$

It follows from Lemma 3.3 that the maximum value above is $\gamma_j = \frac{1}{1+\delta_j}$ and that the maximizer is the eigenfunction corresponding to the eigenvector q^j. That is,

$$u_h^j(x) = \sum_{i=1}^{N_h} q_i^j \phi_i(x)$$

maximizes (3.10).

Referring to the orthogonality condition (3.2), we have

$$\int_{\partial\Omega} \rho(s) T u_h^j(s) T u_h^k(s)\, dS = \sum_{l,m=1}^{N_h} q_l^j q_m^k \int_{\partial\Omega} \rho(s)\phi_j(s)\phi_k(s)\, dS = \left(q^j\right)^T B q^k.$$

It follows from Lemma 3.2 that $Q^T B Q$ is a diagonal matrix. Therefore, under the scaling assumption made

$$\left(q^j\right)^T B q^k = \frac{\delta_{jk}}{1+\delta_j}$$

yielding the desired orthogonality condition. □

3.4. Dimension of the Discrete Eigenspace

We conclude this section by explaining why there are only $M_h = \dim \mathcal{J}_h$ discrete Steklov eigenpairs for a given mesh size h. This assumption has been implicit in the formulation described above.

Lemma 3.4. The generalized eigenvalue problem

$$AQ = BQD \tag{3.17}$$

has at most M_h eigenvectors corresponding to finite eigenvalues. In other words, there exist only M_h discrete Steklov eigenvectors.

Proof. The matrix B is symmetric and clearly has rank at most M_h. □

The conclusion we draw from Lemma 3.4 is that since B is massively rank deficient, the generalized variational principle in terms of the Rayleigh quotient must read

$$\delta_j = \max_{\substack{q^T B q_i = 0 \\ i=1,2,\ldots,j \leqslant M_h \\ q \notin \mathbb{N}(B)}} \frac{q^T A q}{q^T B q}.$$

Thus, once we obtain a basis of $I\!R^{N_h} \setminus \mathbb{N}(B)$ in terms of generalized eigenvectors, any additional eigenvalue will be unbounded. We note that the implicitly restarted Arnoldi method used in ARPACK correctly builds a basis for the complement of $\mathbb{N}(B)$. We provide a few algorithmic details for this process here.

First we note that the implicitly restarted Arnoldi method will converge more quickly to eigenvalues that are large and well separated. However, we are interested in computing the Steklov eigenvalues starting with the smallest and working up. For this reason, we use the shift-invert mode of ARPACK. For the choice of shift $\sigma = -1$, the shifted generalized eigenvalue problem becomes $(A + B)Q = BQ\Gamma$. The relation between the computed eigenvalue γ_i of the shifted problem and the desired Steklov eigenvalue δ_i of the original problem is

$$\gamma_i = \frac{1}{1 + \delta_i}.$$

Therefore, when δ_i is small, γ_i is large. The consequence is that ARPACK can compute the Steklov eigenvalues more quickly by operating on the shifted problem.

Furthermore, since B is expected to have a very large null space, it is important numerically to take care that the eigenvector basis is not corrupted due to a round-off error excitation of this null space. ARPACK operated in the shift-invert mode will automatically deal with this problem. First, the starting vector for the Arnoldi process is forced to lie in the range of the operator $(A + B)^{-1}B$ through multiplication $v_1 \leftarrow (A + B)^{-1}Bv$. This assures all components along null space directions of B have been annihilated.

However, during the course of the implicitly restarted Arnoldi process, round-off can still creep in and corrupt the basis vectors. On convergence, this process will produce a k step Arnoldi factorization

$$(A + B)^{-1}V = VH + fe_k^T,$$

where H is $k \times k$ upper Hessenberg, $V^T BV = I_k$ and e_k is the kth canonical unit vector of length k. Forcing $V^T BV = I_k$ requires multiplication of the basis vectors by B and hence serves to continually purge components in the null space of B.

In order to compute k eigenvalues ARPACK typically requires space for around $2k$ Arnolodi basis vectors. Thus storage is $2nk$ plus a few workspace vectors of length n. If the number of basis vectors is exactly $2k$ then the following describes the computational complexity in terms of floating point operations (flops) for one major iteration of ARPACK:

(1) There are k linear solves $(A+B)w=v$ costing roughly $4n_z$ flops where n_z is the number of non-zeros in the sparse Cholesky factor L where $A+B=LL^T$.
(2) To expand the Arnoldi basis from k to $2k$ in the implicitly restarted Arnoldi scheme requires $6nk^2+\mathcal{O}(n)$ flops.
(3) To contract the basis while keeping the best approximations to desired eigenvalues requires $4nk^2+\mathcal{O}(k^3)$ flops.

Thus, the total cost is on the order of $10nk$ flops plus k linear system solves per major iteration. The Cholesky factorization $(A+B)=LL^T$ is done only once during the entire computation. In these computations, $n=N_h$ and $k=M_h$, and convergence typically requires around 10–20 major iterations.

As a final step, the approximate eigenvectors are "purified" using a scheme suggested by Ericsson and Ruhe [8]. If $Hy=yv$ is an eigenpair for H, an initial approximate generalized eigenpair for (A, B) is given by $x=Vy$ and $\delta=\frac{1}{v}-1$ with approximation error $Ax-Bx\delta=-(A+B)f\frac{e_k^T y}{v}$. This can be improved as follows. Take $\hat{x}=x+f\frac{e_k^T y}{v}$, to be the improved eigenvector approximation. Then it is easily shown that

$$A\hat{x}-B\hat{x}\delta=-Bf\frac{e_k^T y}{v^2}.$$

Since v is typically much larger than one, this gives a far more accurate answer and has the numerical effect of purging components along the null space of B from the eigenvector approximation.

We end this section with the observation that the number of available discrete eigenpairs, which is determined by the dimension of the boundary layer, is dependent on the finite element space used. We recall that for the bilinear finite element space V_{Q_1}, M_h is given by the number of vertices on $\partial\Omega$. In contrast, for the non-conforming finite element space V_{P_h}, M_h is given by the number of element faces in the boundary layer. Therefore, we can obtain more discrete eigenfunctions with the non-conforming finite element space V_{P_h}. Moreover, the boundary error estimate (2.14) indicates that the more eigenpairs we can afford to construct the better approximation results we can expect. Of course, this advantage is offset by the $\mathcal{O}(h)$-approximation capabilities of the non-conforming approximation. This interplay between the mesh size h of the discretization and the number of eigenfunctions computed for the spectral representation plays a key role in determining the approximation error for the elliptic problem. We explore this idea more fully in the computational sections of the paper.

4. STEKLOV EIGENPAIRS ON THE UNIT DISK

For a general domain Ω it is usually not possible to determine an analytic representation of the Steklov eigenpairs satisfying (2.1). However, in the case of the unit disk, such an analytic representation does exist, as we describe in Sec. 4.1. Consequently, we have a unique opportunity to compare our computations from the discrete Steklov spectral method to the actual Steklov eigenpairs on the unit disk. In Sec. 4.2, we present computations performed on the unit disk. We show that the discrete eigenfunctions exhibit the same qualitative behavior as the analytic eigenfunctions, and we demonstrate the success of the discrete Steklov spectral method in approximating the solution of the elliptic problem (1.1). Finally, in Sec. 4.3, we develop an error estimate for the discrete eigenfunctions computed on the unit disk. This in turn leads to an error estimate for the discrete Steklov spectral method. This second estimate is fundamental in that it incorporates both the spatial discretization error and the error resulting from a truncation in the spectral representation.

4.1. Analytic Eigenpairs

In the case of the unit disk, the Steklov eigenfunctions and eigenvalues can be computed using spherical harmonics (see Groemer [9] for details). For simplicity, we assume that $\rho(s)$ is normalized to be constant. The requirement that $\int_{\partial\Omega} \rho(s)\, dS = 1$ dictates that $\rho(s) \equiv \frac{1}{2\pi}$ on the unit circle. We will maintain this value of ρ for the remainder of Sec. 4. It follows that $\delta_0 = 0$ is a simple eigenvalue with corresponding eigenfunction $u^0 = 1$. For $k \geqslant 1$, the Steklov eigenvalues occur in pairs, satisfying

$$\delta_{2k-1} = \delta_{2k} = 2\pi k. \tag{4.1}$$

The corresponding eigenfunctions, in polar coordinates, are

$$u^{2k-1}(r,\theta) = \frac{\sqrt{2}}{\sqrt{1+2\pi k}}\, r^k \sin(k\theta) \text{ and} \tag{4.2}$$

$$u^{2k}(r,\theta) = \frac{\sqrt{2}}{\sqrt{1+2\pi k}}\, r^k \cos(k\theta). \tag{4.3}$$

It is a simple matter to check that the eigenfunctions defined in (4.2) and (4.3) satisfy the theoretical properties outlined in Sec. 2.

First, we note that the Laplacian in polar coordinates is given by

$$\Delta_{r,\theta} u^k(r,\theta) = \frac{1}{r}\frac{\partial}{\partial r}\left(r \frac{\partial u^k}{\partial r}(r,\theta)\right) + \frac{1}{r^2}\frac{\partial^2 u^k}{\partial \theta^2}(r,\theta).$$

The gradient operator in polar coordinates is defined to be

$$\nabla_{r,\theta} u^k(r,\theta) = \left(\frac{\partial u^k}{\partial r}(r,\theta),\ \frac{1}{r}\frac{\partial u^k}{\partial \theta}(r,\theta) \right)^T$$

and the unit normal vector for the unit circle is $n(\theta) = (1,\theta)^T$. At this point, it is easy to verify that the given eigenfunctions do indeed satisfy the Steklov eigenproblem (2.1). Similarly, the weak form of the Steklov eigenvalue problem on the unit disk reads

$$\int_0^1 \int_0^{2\pi} r \nabla_{r,\theta} u^k(r,\theta) \cdot \nabla_{r,\theta} \varphi(r,\theta)\, d\theta\, dr - \frac{\delta_k}{2\pi} \int_0^{2\pi} u^k(1,\theta)\, \varphi(1,\theta)\, d\theta = 0,$$
$$\text{for all } \varphi \in H^1(B(0,1)).$$

We point out that functions in $H^1(B(0,1))$ are defined to be periodic in θ and have periodic first derivatives, a property which we used in deriving the weak formulation.

Finally, one can show that the eigenfunctions on the unit disk satisfy the orthogonality conditions stated in Lemma 2.1. It is worth noting that the eigenfunctions defined by (4.2) and (4.3) are orthogonal on the boundary $\partial\Omega$ and orthonormal on the interior of Ω. In contrast, if we scale the kth eigenfunction by $\sqrt{1+\delta_k}$, then we obtain the eigenfunctions

$$v^{2k-1}(r,\theta) = \sqrt{2}\, r^k \sin(k\theta) \qquad \text{and} \qquad v^{2k}(r,\theta) = \sqrt{2}\, r^k \cos(k\theta).$$

As previously mentioned, these scaled eigenfunctions are orthonormal on the boundary and orthogonal in the interior.

We make a final note that the analytic form of the Steklov eigenpairs presents a simple alternative to the use of Bessel functions. It is well known that Bessel functions are eigenfunctions of the Laplacian on the unit disk [14]. However, the Bessel functions are relatively difficult to enumerate compared to the Steklov eigenfunctions presented here.

4.2. Computations on the Unit Disk

In this section, we present computational results of the discrete Steklov spectral method on the unit disk. To begin, we partition the domain $\Omega = B(0,1)$ into quadrilaterals as shown in Fig. 1(a). The partition shown contains 1280 quadrilaterals, 1313 vertices, and 64 boundary vertices. Hence, there exist 64 discrete Steklov eigenfunctions based on the bilinear approximation, and there exist 256 discrete eigenpairs using the nonconforming harmonic approximation.

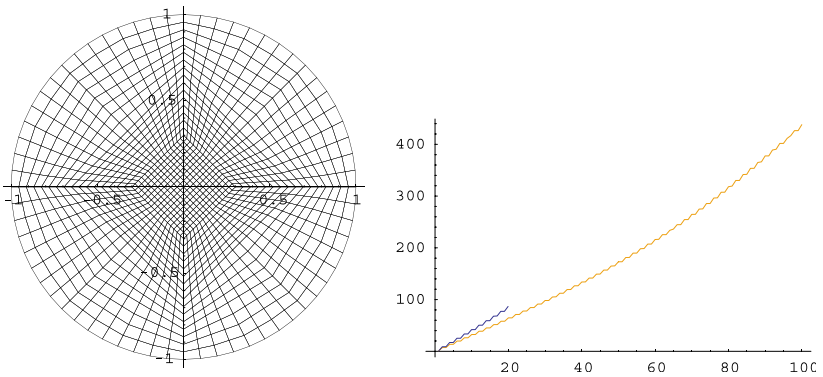

Fig. 1. (a) Partitioning of the unit disk. The partition contains 1280 quadrilaterals, 1313 vertices, and 64 boundary vertices. (b) The yellow curve represents the first 100 discrete eigenvalues computed using the non-conforming harmonic approximation. The gray curve corresponds to the first 20 eigenvalues computed on a coarser mesh.

We compute the discrete eigenvalues by using ARPACK to solve the generalized eigenvalue problem described in Sec. 3. Fig. 1(b) shows the discrete eigenvalues computed with respect to the non-conforming harmonic approximation. The yellow curve corresponds to the first 100 eigenvalues computed on the mesh shown in Fig. 1(a). The gray curve corresponds to the first 20 eigenvalues computed on a coarser mesh. We observe that given a different mesh size, the computed eigenvalues differ slightly. At the same time, the finite element calculations show that, within some tolerance for numerical error, each discrete Steklov eigenvalue has multiplicity two, except for the zero eigenvalue. This corresponds to the analytic form (4.1).

Similarly, we compute the discrete Steklov eigenfunctions with respect to the non-conforming harmonic finite element basis. Plots of the discrete eigenfunctions are shown in Fig. 2 for $k = 2$, 4, 10, and 20. Recalling the analytic formulas (4.2) and (4.3) for the Steklov eigenfunctions on the unit disk, it is clear that, for k large enough, the region of non-trivial support is small and is concentrated close to the boundary. On one hand, neither $\sin(k\theta)$ nor $\cos(k\theta)$ converge strongly to any function as $k \to \infty$. On the other hand, they both converge weakly-$*$ to 0. Therefore, we expect an increasing number of oscillations to be present in the restriction of the eigenfunctions close to the boundary as $k \to +\infty$. Indeed, this is clearly visible in the finite element-based calculations shown in Fig. 2. Moreover, for $k = 10$, Fig. 2(c) shows a function that corresponds to the discrete version of $\sin(2 \times 5\theta)$ on the boundary.

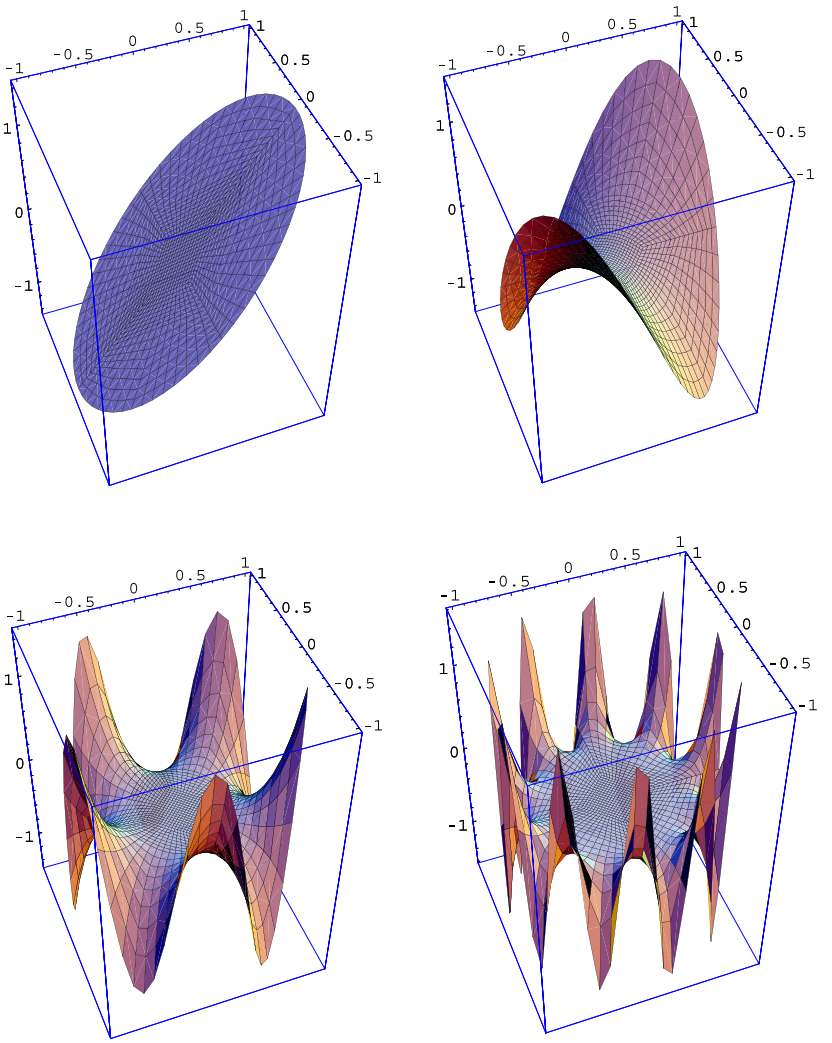

Fig. 2. The plots show the discrete eigenfunctions corresponding to $k = 2$, 4, 10, and 20. The computations are performed using the non-conforming harmonic approximation. As k increases, the region of non-trivial support moves closer to the boundary, and the number of oscillations on the boundary increases.

At this point, we show that application of the discrete Steklov spectral method yields a valid approximate solution to the elliptic problem (1.1). For the computations shown, we impose the boundary data

$$g(x, y) = 25\, x^7\, y^3, \qquad x, y \in \partial B(0, 1). \tag{4.4}$$

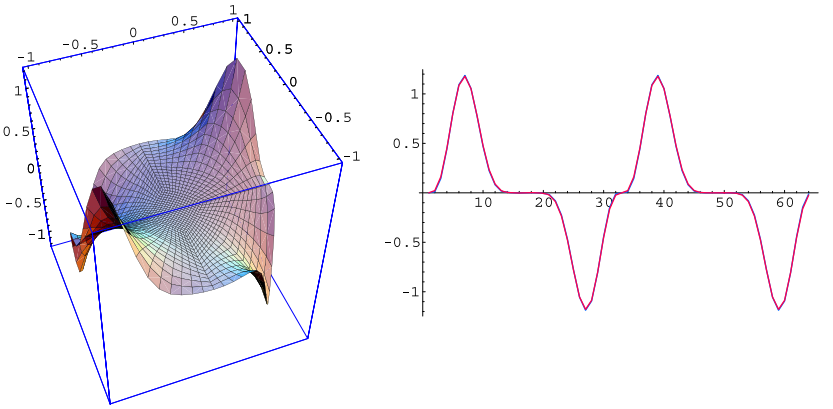

Fig. 3. On the left, the discrete Steklov approximation of the elliptic problem is shown for the given boundary data $g(x, y) = 25x^7 y^3$. The approximation is computed with respect to the non-conforming finite element basis. On the right, the computed and the exact traces of the Dirichlet boundary condition are shown. Both the $L^\infty(\partial B(0, 1))$- and $L^2(\partial B(0, 1))$-errors are on the order of 10^{-2}.

We test both the bilinear and the non-conforming approximation spaces described in Sec. 3. However, the computations that we show here are with respect to the non-conforming approximation. In Fig. 3, the approximate solution $u_h(x, y)$ to the elliptic problem is plotted on the left. On the right, the trace of u_h on the boundary is plotted against the boundary data g prescribed by (4.4). Both the $L^\infty(\partial B(0, 1))$- and $L^2(\partial B(0, 1))$-errors are on the order of 10^{-2}.

4.3. An Error Estimate

In this section, we derive an error estimate for the approximation of the elliptic problem (1.1) computed via the discrete Steklov spectral method. This error estimate is a key improvement on the convergence result in Theorem 2.2 in that we can now estimate the rate of convergence. The approximation error depends on two factors. First, the discrete Steklov eigenfunctions are computed with respect to a particular mesh. Consequently, the resulting approximation error for the eigenfunctions depends on the mesh size h. Second, the approximation to the elliptic problem is written as a Steklov eigenfunction expansion. We know that for a given mesh size, there are M_h available eigenfunctions, where M_h is the dimension of the boundary layer. Typically, we use only $m < M_h$ eigenfunctions, resulting in the truncated expansion

$$u_{m,h}(x) = \sum_{k=1}^{m} c_k u_h^k(x).$$

The second component of the approximation error comes from the truncation error as described in Theorem 2.2. We derive estimates for both the approximation error of the eigenfunctions and the truncation error of the Steklov spectral expansion. Then at the end of this section, we highlight the correlation between these two components of the approximation error through a series of tables.

The error estimates presented in this section are based on the introduction of a norm (4.7) pertaining to the trace spaces $H^s(\partial\Omega)$ (see Auchmuty [2], and Auchmuty and Klouček [3] for complete theory). The novelty of the estimates is in providing the link between the smoothness of the boundary datum in terms of its belonging to a trace space $H^s(\partial\Omega)$ and the truncation error contribution. These estimates show why, typically, only a few, say 10–30, eigenpairs are needed to get a good approximation of the solution to (1.1).

First, we consider the approximation error that occurs when the discrete Steklov eigenfunctions are computed with respect to a particular mesh size h. Recall, the discrete Steklov eigenfunction u_h^k is an approximate solution to the Steklov eigenproblem (2.1) which is a Robin boundary value problem. The standard interpolation error estimate for the conforming bilinear approximation of the Robin problem yields

$$\|u^k - u_h^k\|_{H^1(\Omega)} \leqslant C\,h \tag{4.5}$$

for some constant $C > 0$.

Next, we consider the truncation error obtained when a finite number of exact eigenfunctions is used to represent the solution of the elliptic problem. Let u be the weak solution to the elliptic problem, satisfying Eq. (2), and let

$$u_m(x) = \sum_{k=1}^{m} c_k u^k(x).$$

Then, recalling formula (2.19) from the proof of Theorem 2.2 yields

$$\begin{aligned}
\|u - u_m\|_{H^1(\Omega)}^2 &= \sum_{k=m+1}^{\infty} (1+\delta_k)^2 \left(\int_{\partial\Omega} \rho(s) g(s) T u^k(s)\, dS \right)^2 \\
&= \sum_{k=m+1}^{\infty} (1+\delta_k)^{2+s_0} \\
&\quad \times \int_{\partial\Omega} \rho(s) g(s) T u^k(s)\, dS \frac{1}{(1+\delta_k)^{s_0}} \int_{\partial\Omega} \rho(s) g(s) T u^k(s)\, dS
\end{aligned}$$

for some $s_0 \in \mathbb{R}$. Upon application of the Hölder inequality, we have

$$\|u-u_m\|^2_{H^1(\Omega)} \leqslant \left(\sum_{k=m+1}^{\infty} (1+\delta_k)^{2(2+s_0)} \left(\int_{\partial\Omega} \rho(s) g(s) T u^k(s)\, dS \right)^2 \right)^{1/2} \times \left(\sum_{k=m+1}^{\infty} \frac{1}{(1+\delta_k)^{2s_0}} \left(\int_{\partial\Omega} \rho(s) g(s) T u^k(s)\, dS \right)^2 \right)^{1/2}. \tag{4.6}$$

At this point, we want to relate the truncation error to a trace norm evaluated on the the boundary $\partial\Omega$.

We introduce the trace norm

$$\|g\|^2_{H^s(\partial\Omega)} \stackrel{\text{def}}{=} \sum_{k=0}^{\infty} (1+\delta_k)^{2s+1} \left(\int_{\partial\Omega} \rho(s) g(s) T u^k(s)\, dS \right)^2 \tag{4.7}$$

for some $s \in \mathbb{R}$. For now, we observe that the first term on the right-hand side of (4.6) reduces to $\|g\|_{H^{s_0+3/2}(\partial\Omega)}$. The second term is bounded above by

$$\left(\frac{1}{\left(1+\delta_{m+1}\right)^{2s_0+1}} \sum_{k=m+1}^{\infty} (1+\delta_k) \left(\int_{\partial\Omega} \rho(s) g(s) T u^k(s)\, dS \right)^2 \right)^{1/2} = \frac{1}{\left(1+\delta_{m+1}\right)^{s_0+1/2}} \|g\|_{L^2(\partial\Omega)}.$$

We obtain the definition for the $L^2(\partial\Omega)$-norm either from (2.17) or by taking $s_0 = 0$ in the definition above.

Now, our knowledge of the analytic form of the Steklov eigenpairs on the unit disk gives us an opportunity to further estimate the error with respect to $H^1(B(0,1))$. Recall that, on the unit disk, if $m+1$ is even, then $\delta_{m+1} = \pi(m+1)$, and if $m+1$ is odd, then $\delta_{m+1} = \pi(m+2)$. Either way, we can bound the $m+1$-st eigenvalue below by m. Consequently, we obtain the estimate

$$\|u-u_m\|^2_{H^1(B(0,1))} \leqslant \|g\|_{H^{s_0+3/2}(\partial B(0,1))} \times \frac{1}{(1+m)^{s_0+1/2}} \|g\|_{L^2(\partial B(0,1))}. \tag{4.8}$$

We are now ready to combine the approximation error (4.5) of the discrete eigenfunctions with the truncation error (4.8) of the Steklov spectral expansion.

Consider the overall approximation error for the approximate solution $u_{m,h}(x)$. By combining (4.5) and (4.8), we can write

$$\begin{aligned}\left\|u-u_{m,h}\right\|_{H^1(B(0,1))} &\leqslant \|u-u_m\|_{H^1(B(0,1))}+\left\|u_m-u_{m,h}\right\|_{H^1(B(0,1))}\\ &\leqslant \left(\frac{1}{(1+m)^{s_0+1/2}}\|g\|_{H^{s_0+3/2}(\partial B(0,1))}\|g\|_{L^2(\partial B(0,1))}\right)^{1/2}\\ &\quad +C_1h\\ &\leqslant \left(\frac{1}{(1+m)^{\frac{s_0+1/2}{2}}}+C_2h\right)\|g\|^{1/2}_{H^{s_0+3/2}(\partial B(0,1))}\|g\|^{1/2}_{L^2(\partial B(0,1))}.\end{aligned} \tag{4.9}$$

This error estimate is fundamental for two reasons. First, the estimate is an improvement on the convergence result given in Theorem 2.2 because it provides an estimate on the rate of convergence. Second, the error estimate shows the trade-off between the approximation error that depends on h and the truncation error that depends on m.

For simplicity, we make a particular choice of s_0. Referring back to the computational example presented in Sec. 4.2, the boundary data defined by (4.4) is infinitely continuously differentiable. Therefore, we are justified in taking s_0 as large as we like. For $s_0=1$, the overall approximation error reduces to

$$\left\|u-u_{m,h}\right\|_{H^1(B(0,1))}\leqslant\left(\frac{1}{(1+m)^{3/4}}+C_2h\right)\|g\|^{1/2}_{H^{5/2}(\partial B(0,1))}\|g\|^{1/2}_{L^2(\partial B(0,1))}.$$

For the particular case of the unit disk, this inequality improves upon the two results stated in Theorem 2.2. Namely, the $L^2(\partial\Omega)$ error estimate (2.14) and the $H^1(\Omega)$ convergence result (2.15). First, by the continuous imbedding of $H^1(\Omega)$ into $L^2(\partial\Omega)$ we have

$$\left\|u-u_{m,h}\right\|_{L^2(\partial B(0,1))}\leqslant C\ \left\|u-u_{m,h}\right\|_{H^1(B(0,1))}.$$

Second, the $H^1(\Omega)$ convergence result is augmented by a rate of convergence that depends both on the magnitude of the largest participating eigenvalue and the mesh resolution.

The interplay between the magnitude of the largest participating eigenvalue and the mesh resolution merits some scrutiny. Clearly, as more eigenfunctions are included in the Steklov expansion, i.e., as m increases, the truncation error will decrease. However, improvement in the overall approximation error as m increases is limited by the mesh size h. In particular, if $(1+m)^{-3/4}\leqslant C_2h$, then the overall approximation error will be

dominated by the approximation error of the discrete Steklov eigenfunctions. Hence, we have

$$\|u - u_{m,h}\|_{H^1(B(0,1))} \leqslant C\,h \quad \text{for } (1+m)^{-3/4} \leqslant C_2 h. \tag{4.10}$$

The consequence is that, for a fixed mesh size h, increasing m beyond the point that $(1+m)^{-3/4} \leqslant C_2 h$ yields no real improvement in the overall approximation error. Alternatively, if $(1+m)^{-3/4} \geqslant C_2 h$, then the overall approximation error will be dominated by the truncation error, and we will have

$$\|u - u_{m,h}\|_{H^1(B(0,1))} \leqslant (1+m)^{-3/4} \|g\|^{1/2}_{H^{5/2}(\partial B(0,1))} \|g\|^{1/2}_{L^2(\partial B(0,1))}$$
$$\text{for } (1+m)^{-3/4} \geqslant C_2 h. \tag{4.11}$$

The consequence here is that for a fixed number of eigenfunctions m, there is a certain point beyond which refining the partition does no good to improve the overall approximation error.

It turns out that the relationship (4.10) is clearly evident in the computational results for the example presented in Sec. 4.2 as we illustrate through a series of tables. Tables I–III show the $L^2(\partial\Omega)$-error and $L^\infty(\partial\Omega)$-error for a fixed mesh size h and increasing values of m. The mesh size for each table is $h \approx 0.2$, $h \approx 0.1$, and $h \approx 0.05$, respectively. Examining the tables, we see that the error stagnates for m between 25 and 30 in Table I, for m between 25 and 30 in Table II, and for m between 40 and 80 in Table III. Neglecting the constant C_2 and solving $h \sim (1+m)^{-3/4}$, we would expect the error to stagnate around $m = 7$ for $h = 0.2$, around $m = 20$ for $h = 0.1$, and around $m = 50$ for $h = 0.05$. While these estimates do not predict the exact point of error stagnation, they do provide rough, "order of magnitude" estimates. In order to obtain a more accurate estimate for m we would need more specific knowledge of the constant C_2. One final observation is that the tables show relatively good consistency in the computed spectra between the bilinear and non-conforming harmonic approximation. However, at higher resolutions the bilinear approximation is clearly preferable (cf. Table III).

5. PERFORATED DOMAINS

In this section, we solve the elliptic problem (1.1) on a highly perforated domain. There exists a vast literature dealing with the solution of elliptic equations on perforated domains. Particular topics include homogenization (see Buttazzo [4], Cioranescu and Murat [7], Jikov *et al.* [10],

Table I. Computational results corresponding to the mesh size $h \approx 0.2$. There are 32 boundary DOFs for the bilinear approximation, and there are 65 boundary DOFs for the non-conforming harmonic approximation

Eigenpairs	Predicted $L^2(\partial\Omega)$	Computed $L^2(\partial\Omega)$	Computed $L^\infty(\partial\Omega)$
5	0.27/0.27	0.82/0.82	0.56/0.60
10	0.17/0.17	0.44/0.46	0.37/0.37
15	0.144/0.148	0.36/0.39	0.23/0.33
20	0.113/0.123	0.115/0.237	0.066/0.214
25	0.099/0.10	0.0755/0.221	0.0601/0.201
30	0.094/0.099	0.0754/0.22	0.0593/0.20
60	NA/0.017	NA/0.154	NA/0.140

The error appears to stagnate for m between 25 and 30

Table II. Computational results corresponding to the mesh size $h \approx 0.1$. There are 65 boundary DOFs for the bilinear approximation, and there are 192 boundary DOFs for the nonconforming approximation

Eigenpairs	Predicted $L^2(\partial\Omega)$	Computed $L^2(\partial\Omega)$	Computed $L^\infty(\partial\Omega)$
5	0.27/0.27	0.82/0.82	0.55/0.57
10	0.17/0.17	0.44/0.44	0.37/0.34
15	0.144/0.149	0.357/0.363	0.237/0.262
20	0.122/0.125	0.189/0.125	0.168/0.114
25	0.110/0.11	0.0187/0.0891	0.0158/0.0800
30	0.0963/0.102	0.0187/0.0891	0.0155/0.0806
40	0.0794/0.0884	0.0187/0.0891	0.0155/0.0804
60	0.0624/0.0741	0.0186/0.089	0.0146/0.0812
120	NA/0.0125	NA/0.0721	NA/0.0649

The error appears to stagnate for m between 25 and 30

Table III. Computational results corresponding to the mesh size $h \approx 0.05$. There are 337 boundary DOFs for the conforming approximation, and there are 656 boundary DOFs for the non-conforming approximation

Eigenpairs	Predicted $L^2(\partial\Omega)$	Computed $L^2(\partial\Omega)$	Computed $L^\infty(\partial\Omega)$
5	0.27/0.27	0.82/0.822	0.558/0.567
10	0.113/0.175	0.442/0.442	0.375/0.363
20	0.124/0.125	0.0869/0.0954	0.0507/0.0765
40	0.0863/0.089	0.0046/0.0388	0.00395/0.0359
80	0.0560/0.064	0.00463/0.0388	0.00380/0.0359
120	0.0477 /0.052	0.00463 /0.0353	0.00378/0.0321

The error appears to stagnate for m between 40 and 80

Knyazev and Windlund [12]; scattering, see Piat and Codegone [15]; spectral methods, see Cao and Cui [5]; and the finite element method, see Carstensen and Sauter [6], Strouboulis *et al.* [17]).

The theory of the Steklov eigenpairs developed by Auchmuty and outlined in Sec. 2 requires a simply connected domain. The perforated domain calculations are thus not covered by the presented theory. We found that the Steklov spectral approximation can be applied to non-simply connected domains in the finite dimensional setting.

The finite element approximation of elliptic problems posed on such domains is complicated due primarily to two reasons. First, any refinement of the mesh must take into account the curvature of the voids. Otherwise intersections of mesh elements may occur. Second, the relative distance of the voids is inversely proportional to the smallest eigenvalue of the elliptic operator which in turn is the constant of ellipticity [10]. In other words, the elliptic problem becomes closer to being ill-posed the more closely the voids are spaced. In this section, we show that the discrete Steklov spectral method, with even a moderate discretization, yields results superior to overkill computations in which the finite element approximation is obtained directly with an extremely fine mesh size.

For the calculations we present in this section, we use the Dirichlet boundary data

$$g(x, y) = 2x^7 y^3 \quad (x, y) \in \partial\Omega_p, \tag{5.1}$$

where Ω_p consists of the unit square with 400 evenly spaced circular voids as depicted in Fig. 4. We compute the solution of the elliptic problem using the discrete Steklov spectral method paired with the Q_1 bilinear finite element space. The spatial resolution for this calculation is $h \approx 0.01$, and we use 30 out of an available 7040 Steklov eigenfunctions. The results for this calculation are plotted in Fig. 5. The trace of the computed solution is plotted in blue in comparison with the actual boundary data (5.1) plotted in red. The trace is parametrized by traversing the boundary of the unit square and then traversing the boundary of each perforation in sequence. The computed approximation yields an $H^1(\Omega_p)$-aposteriori error on the order of 0.2.

In Fig. 6, we have plotted the discrete Steklov spectrum on the left and the eigenfunction corresponding to $k = 30$ on the right. As can be seen in Fig. 6(a), the Steklov eigenvalues grow roughly as $13k$. In this case, $(1 + \delta_{30})^{-3/4} \approx 0.01$, and therefore we expect that the overall approximation error is driven by the mesh size, not the number of eigenfunctions used. The eigenfunction in Fig. 6(b) clearly exhibits large oscillations on

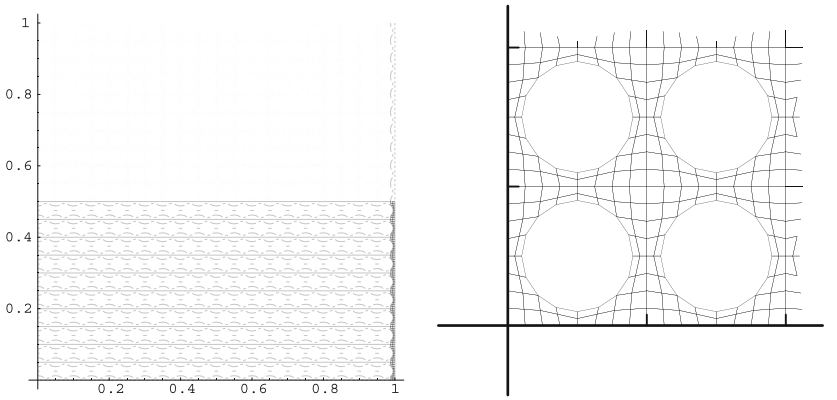

Fig. 4. (a) The unit square containing 400 voids. The computational domain contains 22, 321 nodes, 19, 200 quadrilaterals, and 7040 boundary nodes. (b) A detail of the partitioning of the computational domain into quadrilaterals.

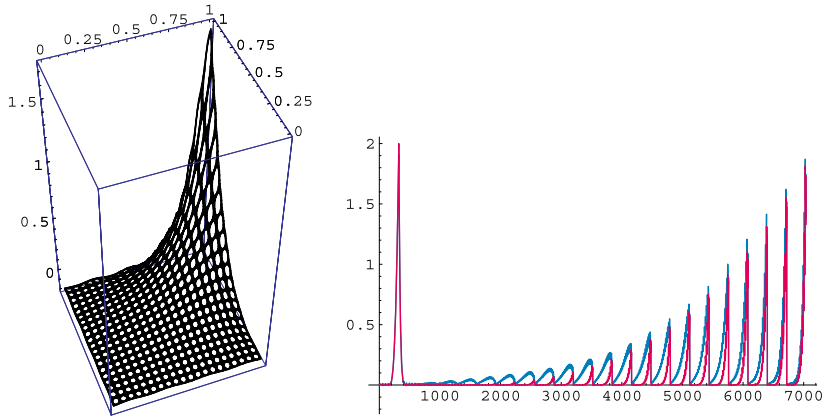

Fig. 5. (a) The bilinear finite element approximation of the solution with the boundary condition $g = 2x^7y^3$. There were 30 out of a possible 7040 Steklov eigenfunctions used in the approximation. (b) The computed trace compared with the trace of the Dirichlet boundary data g. The traces are plotted with respect to a parameterization of the boundary $\partial\Omega_p$. The blue, darker, curve represents the trace of the Steklov solution. The red, lighter, curve is the trace of the boundary data g.

the outer boundary of the perforated domain. However, we were not able to detect any significant oscillations on the boundary of the perforations.

Finally, we compare the approximation from the discrete Steklov spectral method to results that would be expected from an overkill finite element method. Let γ be the smallest distance between two voids in the

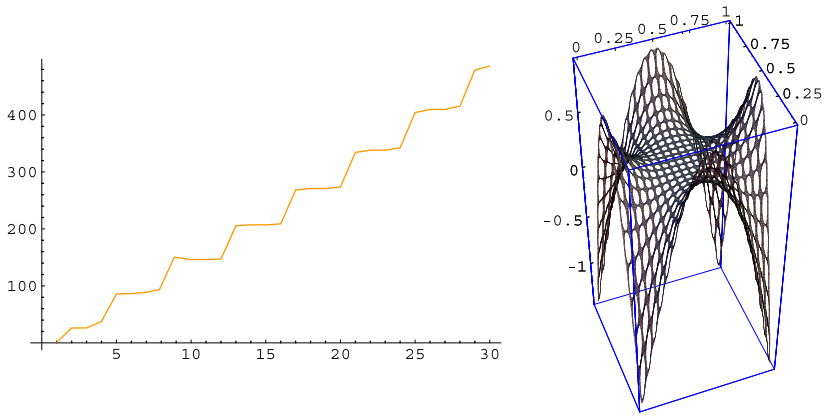

Fig. 6. (a) The yellow curve indicates the Steklov spectrum. The eigenvalues grow roughly as $13k$. The rate of increase becomes higher as the voids are moved closer together. (b) The picture shows the Steklov eigenfunction approximated by the bilinear finite element corresponding to the eigenvalue $k = 30$. The range of the eigenfunction is scaled by 1/5 to enhance visualization.

perforated domain. Then Jikov *et al.* prove that the eigenvalues of the elliptic operator on the perforated domain Ω_p are given by $\gamma^{-2}\lambda_0 + \lambda_k^{\gamma}$ for $k \geqslant 1$ [10]. Here λ_0 is the first eigenvalue of the elliptic problem considered on the corresponding domain without perforation, and the λ_ks are the remaining eigenvalues on the unperforated domain. Furthermore, Cao and Cui prove that, for a direct finite element application, the $H^2(\Omega_p)$-error is on the order of γ^{-2}, [Theorem 3.3, [5]]. By application of Cea's Lemma, we have the finite element error estimate

$$\|u - u_h\|_{H^1(\Omega_p)} \leqslant Ch\|u\|_{H^2(\Omega_p)} \approx C\frac{h}{\gamma^2}.$$

Therefore, the approximation properties of the finite element solution deteriorate as $\gamma \to 0_+$.

In order to make a more direct comparison between the Steklov solution and the finite element solution on perforated domains, we consider a less complex problem. Let Ω_{p4} be the unit square with 4×4 evenly distributed circular voids, and let

$$g_4(x, y) \stackrel{\text{def}}{=} \sin^2(5xy), \quad (x, y) \in \partial\Omega_{p4}. \tag{5.2}$$

The corresponding γ for the domain Ω_{p4} is equal to 0.1. We perform calculations on five staggered grids obtained by uniformly subdividing the coarse grid similar to the one shown in Fig. 4(b). We denote by i the

Table IV. The table indicates that, based on a rough estimate of the approximation error given by h/γ^2 the finite element solution can have at most one decimal place of accuracy

i	h_i (approx.)	# DOFs	Eigenpairs	h_i/γ^2
0	0.08	273	192	8
1	0.04	945	384	4
2	0.02	3441	768	2
3	0.01	13041	1536	1
4	0.005	50673	3072	0.5
5	0.0025	199665	6144	0.25

number of refinements to the coarse mesh. Then Table IV summarizes the various spatial resolutions h_i along with the corresponding number of equations, number of available eigenpairs, and a rough estimate of the expected error for standard finite element calculations. We were unable to generate more than five mesh refinements without having overlapping elements due to the curvature of the voids.

For a given mesh size, we would like to compare the accuracy of the finite element solution to the accuracy of the Steklov approximation. However, on the perforated domain, we do not know the true solution to the elliptic problem. Therefore, we treat the finite element solution u_{h_5} corresponding to the mesh size h_5 as the "exact" solution. Then our measure of accuracy is provided by $\|u_{h_i} - \Pi_{h_i} u_{h_5}\|_{H_0^1(\Omega_{p4})}$. Here Π_{h_i} is the projection of the fine grid solution onto a coarser grid.

All of the calculations that we made were based on the bilinear finite element space V_{Q_1}. For the Steklov spectral approximations, we used a fixed number of 50 eigenpairs. Fig. 7 shows the performance of the Steklov approximation compared to the finite element solution. This figure indicates that even a moderate discretization of the perforated domain, in combination with the Steklov approximation, yields results that can be viewed as qualitatively more accurate than the standard finite element approximation. Finally, we note that

$$\|u_{h_4} - \Pi_{h_4} u_{h_5}\|_{H_0^1(\Omega_{p4})} \approx 6.6 \times 10^{-4}.$$

Comparing the above difference in the H_0^1-norm with the expected approximation error, we conclude that obtaining a highly accurate solution would require even more then five refinements of the original grid.

In the presented implementation, the computation of the Steklov eigenpairs is based on a finite element discretization. The direct finite element based calculation of the solution to (1.1) provides the best

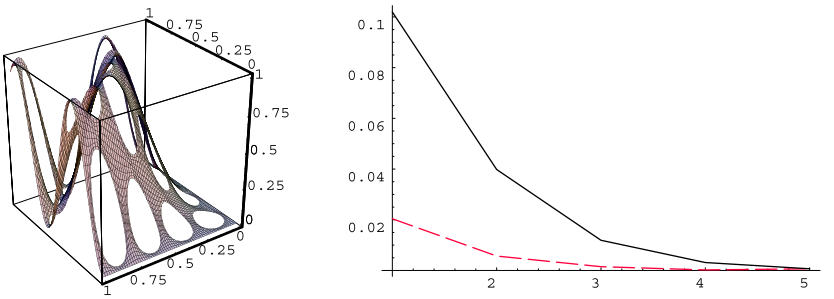

Fig. 7. (a) Plot of the discrete solution for the boundary condition (5.2). (b) The curves show convergence rates to the "exact" solution u_{h_5}. The solid curve indicates the approximation error for the finite element approximation while the dashed curve indicates the approximation error for the discrete Steklov spectral approximation. The x-axis shows the number of uniform mesh refinements.

approximation to the true solution in the energy norm, i.e., in the H^1- seminorm in our case of the Laplacian. Hence, we should conclude that the approximation obtained by the Steklov spectral approximation cannot be more accurate when the performance is measured in the energy norm. However, this contradicts the result shown at the right plot in Fig. 7, which indicates much better performance especially at low resolution.

In order to reconcile this discrepancy, we offer the following argument. The error in the energy norm for the direct finite element computations behaves, roughly, as h/γ^2. On the other hand, the numerical computations suggest that $\|u_m - u_{m,h}\|_{H^1(B(0,1))} \sim h/(\delta_1^2 \delta_m)$. Recall that $\delta_0 = 0$, $\delta_1 \sim \gamma$. This may be a consequence of the fact that the Steklov eigenfunctions are nearly trivial inside the computational domain but oscillate rapidly on (and close to) the boundary. Thus one would conjecture that $\|u_m - u_{m,h}\|_{H^1(B(0,1))} \sim h/\gamma$ for large frequences, which correlates with Fig. 7.

6. CONCLUSION

In this paper, we have shown that the discrete Steklov spectral method is effective for approximating solutions to certain elliptic boundary value problems. We conclude by discussing three areas in which this method could prove useful. First, it is our experience that only a few Steklov eigenpairs are needed to get a sufficiently accurate solution to problem (1.1). In addition, the computational work required to obtain these eigenpairs is comparable to the work of implementing the finite element method. However, for the discrete Steklov spectral method, the solution

$u(x)$ depends on the boundary data g only through the coefficients c_j. Since the coefficients are cheap to compute, this method should be suitable for repeatedly solving problem (1.1) with a number of different boundary data g. Second, solutions to elliptic problems can be represented simply by the coefficients of the Steklov spectral expansion. This data-sparse representation can potentially be used for model reduction problems or as part of optimization or control problems. Finally, the Steklov spectral method provides a solvability criterion for (1.1) in terms of the summability of the coefficients c_j. In fact, we use this summability condition to define the trace space $H^{1/2}(\partial\Omega)$, and this definition yields a natural generalization to trace spaces in different topologies [2]. The discrete Steklov spectral method can be used to generate *generalized harmonic functions* which "solve" the Laplace equation when the boundary data g is not in $H^{1/2}(\partial\Omega)$. This concept is explored in detail by Auchmuty and Klouček [3].

Several workers, including also one of the referees of our manuscript, mentioned a possible connection between the presented Steklov spectral approach and the boundary element method (see e.g., Wendland [18]).

ACKNOWLEDGMENTS

The first author was supported in part by the grants NSF DMS–0107539, NSF Grant ACI-0325081, the grant NSF Grant CCR-0306503, and by the grant MEXC-CT-2005-023843 from the European Commission. The second author was supported in part by the grants NSF Grant ACI-0325081 and NSF Grant CCR-0306503. The third author was supported in part by the grant NASA SECTP NAG5–8136. All authors were supported in part by the Los Alamos National Laboratory Computer Science Institute (LACSI) through LANL contract number 03891–99–23, as part of the prime contract W–7405–ENG-36 between the Department of Energy and the Regents of the University of California.

REFERENCES

1. Auchmuty, G., (2004). Steklov Eigenproblems, and representation of solutions of elliptic, boundary value problems. Num. Func. Anal. Opt. **25** no. (3-4), 321–348.
2. Auchmuty, G., (2005). Spectral characterization of the trace, spaces $H^s(\partial\Omega)$, *SIAM J. Math. Anal.* (in Press).
3. Auchmuty, G., and Klouček, P. (2006). Generalized harmonic, functions, and the dewetting of thin films. *App Math. Opt.* (in Press).
4. Buttazzo, G. On the existence of minimizing domains for some shape optimization problems, ESAIM: Proceedings Actes du 29éme Congrés d'Analyse Numérique **3** (1998), 51–64.

5. Cao, L.-Q., and Cui, J.-Z. (2004). Assymptotic expansions and numerical algorithms of eigenvalues and eigenfunctions of the Dirichlet problem for the second order elliptic equations in perforated domains. *Numer. Math*. **96**(3), 525–581.
6. Carstensen, C., and Sauter, S. A. (2001). A posteriori error analysis for elliptic PDEs on domains with complicated structures. *Math. Comp*. to appear.
7. Cioranescu, D., and Murat, F. (1997). Topics in the mathematical modelling of composite materials, A. Cherkaev (ed.), Prog. Nonlinear Differ. Equ. Appl., ch. A strange term coming from nowhere, pp. 45–93, Birkhaüser.
8. Ericsson, T., and Ruhe, A. (1980). The spectral transformation Lanczos method for the numerical solution of large sparse generalized symmetric eigenvalue problems. *Math. of Comp*. **35**(152), 1251–1268.
9. Groemer, H. (1996). Geometric applications of Fourier series and spherical harmonics, Cambridge University Press, Cambridge.
10. Jikov, V. V., Kozlov, S. M., and Olejnik, O. A. (1994). Homogenization of differential operators and integral functionals, Springer-Verlag, Berlin.
11. Klouček, P., Li, B., and Luskin, M. (1996). Analysis of a class of nonconforming finite elements for crystalline microstructures. *Math. Comp*. **65**(215), 1111–1135.
12. Knyazev, A., and Windlund, O. (2001). Lavrentiev regularization + Ritz approximation = Uniform finite element error estimates for differential equations with rough coefficients. *Math. Comp*.
13. Lehoucq, R. B., Sorensen, D. C., and Yang, C. (1998). ARPACK users' guide: Solution of large-scale eigenvalue problems with implicitly restarted Arnoldi methods, SIAM, Philadelphia.
14. Magenes, E., and Lions, J. L. (1968). Problèmes aux limites non homogènes et applications, *Dunod, Paris*.
15. Piat, V. Ch., and Codegone, M. (2003). Scattering problem in a domain with small holes. *Rev. R. Acad. Cien. Serie A., Mat*. **97**(3), 447–454.
16. Sorensen, D. C. (1992). Implicit application of polynomial filters in a k-step Arnoldi method. SIAM J. *Matrix. Anal. Appl*. **13**, 357–385.
17. Strouboulis, T., Zhang, L., and Babuška, I. (2004). *p*-version of the generalized FEM using mesh-based handbooks with applications to multiscale problems.
18. Wendland, W. L. (1999). Mathematical Aspects of Boundary Element Methods, CRC Research Notes in Mathematics (Paperback), Chapman & Hall.